J. Fluid Mech. (2012), *vol.* 706, *pp.* 150–172.
doi:10.1017/jfm.2012.242

On freely decaying, anisotropic, axisymmetric Saffman turbulence

P. A. Davidson[1]†, N. Okamoto[2] and Y. Kaneda[3]

[1] Department of Engineering, University of Cambridge, Trumpington Street, Cambridge CB2 1PZ, UK

[2] Centre for Computational Science, Nagoya University, Nagoya 464-8603, Japan

[3] Department of Computational Science & Engineering, Nagoya University, Nagoya 464-8603, Japan

(Received 22 August 2011; revised 4 April 2012; accepted 21 May 2012;
first published online 2 July 2012)

We consider freely decaying, anisotropic, statistically axisymmetric, Saffman turbulence in which $E(k \to 0) \sim k^2$, where E is the energy spectrum and k the wavenumber. We note that such turbulence possesses two statistical invariants which are related to the form of the spectral tensor $\Phi_{ij}(\boldsymbol{k})$ at small k. These are $M_\parallel = \Phi_\parallel(k_\parallel = 0, k_\perp \to 0)$ and $M_\perp = 2\Phi_\perp(k_\parallel = 0, k_\perp \to 0)$, where the subscripts $\parallel$ and $\perp$ indicate quantities parallel and perpendicular to the axis of symmetry. Since $M_\parallel \sim u_\parallel^2 \ell_\perp^2 \ell_\parallel$ and $M_\perp \sim u_\perp^2 \ell_\perp^2 \ell_\parallel$, u and ℓ being integral scales, self-similarity of the large scales (when it applies) demands $u_\parallel^2 \ell_\perp^2 \ell_\parallel =$ constant and $u_\perp^2 \ell_\perp^2 \ell_\parallel =$ constant. This, in turn, requires that $u_\parallel^2/u_\perp^2$ is constant, contrary to the popular belief that freely decaying turbulence should exhibit a 'return to isotropy'. Numerical simulations performed in large periodic domains, with different types and levels of initial anisotropy, confirm that $M_\parallel$ and $M_\perp$ are indeed invariants and that, in the fully developed state, $u_\parallel^2/u_\perp^2 =$ constant. Somewhat surprisingly, the same simulations also show that $\ell_\parallel/\ell_\perp$ is more or less constant in the fully developed state. Simple theoretical arguments are given which suggest that, when $u_\parallel^2/u_\perp^2$ and $\ell_\parallel/\ell_\perp$ are both constant, the integral scales should evolve as $u_\perp^2 \sim u_\parallel^2 \sim t^{-6/5}$ and $\ell_\perp \sim \ell_\parallel \sim t^{2/5}$, irrespective of the level of anisotropy and of the presence of helicity. These decay laws, first proposed by Saffman (*Phys. Fluids*, vol. 10, 1967, p. 1349), are verified by the numerical simulations.

Key words: homogeneous turbulence, turbulence simulation, turbulence theory

1. Introduction: Saffman's analysis and its experimental verification

Saffman established the key properties of freely decaying, homogeneous, incompressible turbulence in which the energy spectrum, $E(k)$, takes the form $E(k \to 0) \sim k^2$, k being the wavenumber (Saffman 1967*a*). This is important as $E(k \to 0) \sim k^2$ is thought to be one of two canonical cases in homogeneous turbulence, the other being $E(k \to 0) \sim k^4$, as discussed in Batchelor & Proudman (1956). (See also Krogstad & Davidson 2010; Davidson 2009, 2011, who discuss the properties of $E \sim k^2$ versus $E \sim k^4$ turbulence, as well as why these two particular spectra are the most likely to be observed in practice.) The early wind tunnel experiments of Bennett & Corssin (1978), as well as the numerical simulations of Ishida, Davidson

† Email address for correspondence: pad3@eng.cam.ac.uk

& Kaneda (2006), show clear evidence of $E(k \to 0) \sim k^4$ turbulence, while the recent wind tunnel experiments of Krogstad & Davidson (2010) provide the first clear-cut experimental evidence of $E(k \to 0) \sim k^2$ turbulence. These two classes of flow exhibit quite different energy decay characteristics and which type is observed depends on the way in which the turbulence is initiated. As noted by Saffman (1967*a*) (see also Davidson 2009, 2010; Krogstad & Davidson 2010), if the turbulent eddies possess a significant amount of linear impulse at $t = 0$, then the subsequent flow has an $E \sim k^2$ energy spectrum, whereas a lack of linear impulse in the initial condition leads to $E \sim k^4$. In this paper we focus on Saffman turbulence, in which $E(k \to 0) \sim k^2$ and a typical eddy possesses a significant amount of linear impulse, $(1/2)\int \boldsymbol{x} \times \boldsymbol{\omega}\, \mathrm{d}V$, where $\boldsymbol{\omega} = \boldsymbol{\nabla} \times \boldsymbol{u}$ is the vorticity field.

The case of isotropic Saffman turbulence is well documented. Here we have

$$E(k \to 0) = \frac{Lk^2}{4\pi^2} + O(k^4), \quad L = \int \langle \boldsymbol{u} \cdot \boldsymbol{u}' \rangle \, \mathrm{d}\boldsymbol{r}, \tag{1.1}$$

where L is known as Saffman's integral and $\langle \boldsymbol{u} \cdot \boldsymbol{u}' \rangle = \langle \boldsymbol{u}(\boldsymbol{x}) \cdot \boldsymbol{u}(\boldsymbol{x} + \boldsymbol{r}) \rangle$. Noting that

$$\langle \boldsymbol{u} \cdot \boldsymbol{u}' \rangle = \frac{1}{r^2} \frac{\partial}{\partial r} (r^3 u^2 f), \tag{1.2}$$

where $u^2 = (1/3)\langle \boldsymbol{u^2} \rangle$ and $f(r)$ is the usual longitudinal correlation function, defined by $u^2 f(r) = \langle u_x(\boldsymbol{x}) u_x(\boldsymbol{x} + r\hat{\boldsymbol{e}}_x) \rangle$, we have

$$L = 4\pi \, [r^3 u^2 f]_\infty, \tag{1.3}$$

where the subscript ∞ indicates $r \to \infty$. Thus $f_\infty \sim r^{-3}$ in Saffman turbulence.

Saffman also showed that L is an invariant of the motion. This follows directly from the Kármán–Howarth equation

$$\frac{\partial}{\partial t} \langle \boldsymbol{u} \cdot \boldsymbol{u}' \rangle = \frac{1}{r^2} \frac{\partial}{\partial r} \frac{1}{r} \frac{\partial}{\partial r} (r^4 u^3 K) + 2\nu \nabla^2 \langle \boldsymbol{u} \cdot \boldsymbol{u}' \rangle \tag{1.4}$$

and the observation that the longitudinal triple correlation, $u^3 K(r) = \langle u_x^2(\boldsymbol{x}) u_x(\boldsymbol{x} + r\hat{\boldsymbol{e}}_x) \rangle$, decays with separation as $K_\infty \leqslant O(r^{-4})$ in isotropic turbulence (Batchelor & Proudman 1956). The invariance of L, combined with self-similarity of the large scales, then yields

$$u^2 \ell^3 = \text{constant}, \tag{1.5}$$

where ℓ is a suitably defined integral scale. This may be combined with the empirical but well-established relationship

$$\frac{\mathrm{d}u^2}{\mathrm{d}t} = -A \frac{u^3}{\ell}, \quad A \approx \text{constant}, \tag{1.6}$$

to yield the decay laws

$$\frac{u^2}{u_0^2} = \left[1 + \frac{5A}{6} \left(\frac{u_0 t}{\ell_0} \right) \right]^{-6/5}, \tag{1.7}$$

$$\frac{\ell}{\ell_0} = \left[1 + \frac{5A}{6} \left(\frac{u_0 t}{\ell_0} \right) \right]^{2/5}, \tag{1.8}$$

where u_0 and ℓ_0 are the initial values of u and ℓ (Saffman 1967*b*). Expression (1.5) was confirmed in the grid turbulence experiments of Krogstad & Davidson

(2010), though the corresponding energy decay exponent in $u^2 \sim t^{-m}$ was found to be fractionally smaller than $m = 6/5$, which was traced back to a slow temporal decline in the coefficient A. The reason for the slow decline of A in these experiments is not yet understood, though it may be linked to the slight inhomogeneity of the turbulence, or else to the slow decline in Reynolds number as the turbulence decays. Expressions (1.5)–(1.8) have yet to be confirmed in direct numerical simulations (though see the large-eddy simulations of Chasnov 1995), and this constitutes one of the purposes of this paper, the other being to explore the effects of anisotropy.

The anisotropic case was explored in depth by Saffman (1967*a*). Here we find that the spectral tensor (the transform of $\langle u_i u_j' \rangle = \langle u_i(\boldsymbol{x}) u_j(\boldsymbol{x}+\boldsymbol{r}) \rangle$) takes the form

$$\Phi_{ij}(\boldsymbol{k} \to 0) = M_{\alpha\beta} \left\{ \delta_{i\alpha} - \frac{k_i k_\alpha}{k^2} \right\} \left\{ \delta_{j\beta} - \frac{k_j k_\beta}{k^2} \right\} + O(k), \tag{1.9}$$

where $M_{\alpha\beta}$ is symmetric, independent of $\boldsymbol{k}$, and related to the second moment of the two-point vorticity correlation, $\langle \omega_i \omega_j' \rangle$, by

$$(2\pi)^3 M_{ij} = \frac{1}{2}\Omega_{ij} - \frac{1}{4}\delta_{ij}\Omega_{kk}, \quad \Omega_{ij} = \int r^2 \langle \omega_i \omega_j' \rangle \, \mathrm{d}\boldsymbol{r}, \tag{1.10}$$

or equivalently,

$$\Omega_{ij} = (2\pi)^3 [2M_{ij} - 2\delta_{ij} M_{kk}]. \tag{1.11}$$

The corresponding energy spectrum is $E(k) = (4/3)\pi M_{\alpha\alpha} k^2 + O(k^3)$, and the long-range velocity correlations corresponding to (1.9) turn out to be

$$\langle u_i u_j' \rangle_\infty = -M_{\alpha\beta}\pi^2 \left\{ \delta_{i\alpha}\nabla^2 - \frac{\partial^2}{\partial r_i \partial r_\alpha} \right\} \left\{ \delta_{j\beta}\nabla^2 - \frac{\partial^2}{\partial r_j \partial r_\beta} \right\} r, \tag{1.12}$$

where $r = |\boldsymbol{r}| = |\boldsymbol{x}' - \boldsymbol{x}|$. Hence $\langle u_i u_j' \rangle_\infty \sim O(r^{-3})$, which is consistent with (1.3). The source of these r^{-3} tails in the two-point velocity correlations is the Biot-Savart law, in which an eddy with finite linear impulse induces irrotational far-field velocity fluctuations of order r^{-3} (see, for example, Davidson 2004, p. 633). This leads directly to the long-range correlations $\langle u_i u_j' \rangle_\infty \sim O(r^{-3})$ and $\langle u_i u_j u_k' \rangle_\infty \sim O(r^{-3})$, except in isotropic turbulence, where symmetry kills the leading-order term in $\langle u_i u_j u_k' \rangle_\infty$, leaving $\langle u_i u_j u_k' \rangle_\infty \sim O(r^{-4})$. These far-field fluctuations are, however, irrotational and so do not contribute to $\langle \omega_i \omega_j' \rangle_\infty$, which are of order $\langle \omega_i \omega_j' \rangle_\infty \leqslant O(r^{-6})$, rather than the $\langle \omega_i \omega_j' \rangle_\infty = O(r^{-5})$ scaling that (1.12) might imply. It follows that the Ω_{ij} defined by (1.10) are absolutely convergent, and by implication the M_{ij} are well defined. By contrast, the integrals

$$L_{ij} = \lim_{V\to\infty} \int_V \langle u_i u_j' \rangle \, \mathrm{d}\boldsymbol{r} \tag{1.13}$$

are convergent (i.e. independent of the size of V), but only conditionally convergent, since their values depend on the shape of the volume whose surface recedes to infinity. Note that, since $\boldsymbol{u}$ is solenoidal, we may rewrite L_{ij} as a surface integral,

$$L_{ij} = \lim_{V\to\infty} \int_V \langle u_i u_j' \rangle \, \mathrm{d}\boldsymbol{r} = \lim_{S\to\infty} \oint \langle u_i u_k' \rangle_\infty r_j \, \mathrm{d}\boldsymbol{S}_k, \tag{1.14}$$

$\mathrm{d}\boldsymbol{S}$ being the surface element. It follows that the integrals L_{ij} are uniquely determined by $\langle u_i u_j' \rangle_\infty$, and hence by M_{ij}. For the particular case of a spherical volume,

Saffman (1967*a*) established that

$$L_{ij} = (2\pi)^3[\tfrac{7}{15}M_{ij} + \tfrac{1}{15}\delta_{ij}M_{kk}] = \tfrac{7}{30}\Omega_{ij} - \tfrac{2}{15}\delta_{ij}\Omega_{kk}. \tag{1.15}$$

Saffman also suggested that L_{ij}, and by implication M_{ij} and Ω_{ij}, are invariants of the motion. Although his arguments are non-rigorous, because they rely on a loose application of the central-limit theorem, they are nevertheless highly suggestive, and indeed Davidson (2010) provides an independent proof of $L_{ij} = \text{constant}$.

In summary, then, there is a well-developed theory of freely decaying Saffman turbulence, and this is important because it constitutes one of the two canonical cases in homogeneous turbulence. Some predictions, such as $u^2 \sim t^{-6/5}$ in isotropic turbulence, have been verified by experiment. Others, such as $L_{ij} = \text{constant}$ in anisotropic turbulence, have not been verified. The purpose of this paper is to put the various predictions to the test, and to investigate the influence of anisotropy on the decay of energy. For simplicity, we restrict ourselves to statistically axisymmetric turbulence.

2. Statistically axisymmetric Saffman turbulence

In this section we focus on statistically axisymmetric turbulence, expanding on the discussion in Davidson (2010). We take the axis of symmetry to be the z-axis and use subscripts $\parallel$ and $\perp$ to indicate quantities parallel and perpendicular to the symmetry axis. Thus, for example,

$$\Phi_\parallel = \Phi_{zz}, \quad \Phi_\perp = \Phi_{xx} + \Phi_{yy}, \quad L_\parallel = L_{zz}, \quad L_\perp = L_{xx} + L_{yy},$$

and so on. Now in axisymmetric turbulence (which includes reflectional symmetry) Φ_{ij} takes the form

$$\Phi_{ij} = (F+G)[k^2\delta_{ij} - k_ik_j] - G[k_\parallel^2\delta_{ij} + k^2\lambda_i\lambda_j - k_\parallel(k_i\lambda_j + k_j\lambda_i)], \tag{2.1}$$

where $\boldsymbol{\lambda}$ is a unit vector parallel to the symmetry axis and F and G are even functions of $k = |\boldsymbol{k}|$ and $k_\parallel$. Thus, for example, if $i \neq j$ then

$$\Phi_{ij}(k_\parallel = 0) = -(F+G)k_ik_j. \tag{2.2}$$

Comparing (2.2) with (1.9) we see that $M_{ij} = 0$ if $i \neq j$, and its only non-zero components are $M_\parallel$ and $M_{xx} = M_{yy} = (1/2)M_\perp$. Similarly, (1.11) tells us that $\Omega_{ij} = 0$ if $i \neq j$, and so (1.10) and (1.11) reduce to

$$(2\pi)^3 M_\parallel = \tfrac{1}{4}[\Omega_\parallel - \Omega_\perp], \quad (2\pi)^3 M_\perp = -\tfrac{1}{2}\Omega_\parallel, \tag{2.3}$$

and

$$\Omega_\perp = -(2\pi)^3[2M_\perp + 4M_\parallel], \tag{2.4}$$

where $M_\parallel$ and $M_\perp$, or equivalently $\Omega_\parallel$ and $\Omega_\perp$, are the invariants of axisymmetric Saffman turbulence. The most general form of $\Phi_{ij}(k \to 0)$ is then

$$\Phi_\parallel = M_\parallel\frac{k_\perp^4}{k^4} + \frac{1}{2}M_\perp\frac{k_z^2k_\perp^2}{k^4} + O(k), \tag{2.5}$$

$$\Phi_\perp = M_\parallel\frac{k_z^2k_\perp^2}{k^4} + \frac{1}{2}M_\perp\left[1 + \frac{k_z^4}{k^4}\right] + O(k), \tag{2.6}$$

$$\Phi_{xy} = M_\parallel\frac{k_xk_yk_z^2}{k^4} - \frac{1}{2}M_\perp\frac{k_xk_y}{k^2}\left[1 + \frac{k_z^2}{k^2}\right] + O(k), \tag{2.7}$$

$$\Phi_{xz} = -M_{\parallel}\frac{k_x k_z k_\perp^2}{k^4} - \frac{1}{2}M_\perp \frac{k_x k_z^3}{k^4} + O(k), \tag{2.8}$$

$$\Phi_{yz} = -M_{\parallel}\frac{k_y k_z k_\perp^2}{k^4} - \frac{1}{2}M_\perp \frac{k_y k_z^3}{k^4} + O(k), \tag{2.9}$$

where $k_\perp^2 = k^2 - k_z^2$. It follows that (Davidson 2010)

$$M_{\parallel} = \Phi_{\parallel}(k_z = 0, k_\perp \to 0) = (2\pi)^{-3}\lim_{k_\perp\to 0}\int \mathrm{e}^{-j\boldsymbol{k}_\perp\cdot\boldsymbol{r}_\perp}\langle u_{\parallel}u'_{\parallel}\rangle\,\mathrm{d}\boldsymbol{r} = \text{constant}, \tag{2.10a}$$

$$\Phi_{\parallel}(k_\perp = 0, k_z \to 0) = (2\pi)^{-3}\lim_{k_z\to 0}\int \mathrm{e}^{-jk_z r_z}\langle u_{\parallel}u'_{\parallel}\rangle\,\mathrm{d}\boldsymbol{r} = 0, \tag{2.10b}$$

$$\frac{1}{2}M_\perp = \Phi_\perp(k_z = 0, k_\perp \to 0) = (2\pi)^{-3}\lim_{k_\perp\to 0}\int \mathrm{e}^{-j\boldsymbol{k}_\perp\cdot\boldsymbol{r}_\perp}\langle \boldsymbol{u}_\perp\cdot\boldsymbol{u}'_\perp\rangle\,\mathrm{d}\boldsymbol{r} = \text{constant}, \tag{2.11a}$$

and

$$M_\perp = \Phi_\perp(k_\perp = 0, k_z \to 0) = (2\pi)^{-3}\lim_{k_z\to 0}\int \mathrm{e}^{-jk_z r_z}\langle \boldsymbol{u}_\perp\cdot\boldsymbol{u}'_\perp\rangle\,\mathrm{d}\boldsymbol{r} = \text{constant}, \tag{2.11b}$$

which provide alternative definitions of $M_{\parallel}$ and $M_\perp$ to (2.3). Note that these conservation laws also apply to the less restrictive case of helical axisymmetric turbulence which lacks reflectional symmetry, as shown in Davidson (2010), Appendix B. These key conservation laws will be verified in our numerical simulations.

The far-field correlations corresponding to (2.5)–(2.9) are, from (1.12),

$$\langle u_z u'_z\rangle_\infty = -\pi^2\left[M_{\parallel}\nabla_\perp^4(r) + \tfrac{1}{2}M_\perp\nabla_\perp^2\nabla_{\parallel}^2(r)\right], \tag{2.12}$$

$$\langle \boldsymbol{u}_\perp\cdot\boldsymbol{u}'_\perp\rangle_\infty = -\pi^2\left[M_{\parallel}\nabla_\perp^2\nabla_{\parallel}^2(r) + \tfrac{1}{2}M_\perp\nabla_{\parallel}^4(r)\right], \tag{2.13}$$

$$\langle u_{r_\perp}u'_z\rangle_\infty = \pi^2\left[M_{\parallel}\nabla_\perp^2 + \tfrac{1}{2}M_\perp\nabla_{\parallel}^2\right]\frac{\partial^2 r}{\partial r_z\partial r_\perp}, \tag{2.14}$$

where

$$\nabla_{\parallel}^4(r) = -\frac{3}{r^3} + 3\frac{r_z^2}{r^5} + 15\frac{r_z^2 r_\perp^2}{r^7}, \quad \nabla_\perp^4(r) = \frac{1}{r^3} - 9\frac{r_z^2}{r^5} + 15\frac{r_z^2 r_\perp^2}{r^7}, \tag{2.15}$$

$$\nabla_{\parallel}^2\nabla_\perp^2(r) = \frac{1}{r^3} + 3\frac{r_z^2}{r^5} - 15\frac{r_z^2 r_\perp^2}{r^7}, \tag{2.16}$$

and

$$\nabla_{\parallel}^2\frac{\partial^2 r}{\partial r_z\partial r_\perp} = -6\frac{r_z r_\perp}{r^5} + 15\frac{r_z r_\perp^3}{r^7}, \quad \nabla_\perp^2\frac{\partial^2 r}{\partial r_z\partial r_\perp} = -3\frac{r_z r_\perp}{r^5} + 15\frac{r_z^3 r_\perp}{r^7}. \tag{2.17}$$

(Note that we have used $\nabla_{\parallel}^4(r) + 2\nabla_{\parallel}^2\nabla_\perp^2(r) + \nabla_\perp^4(r) = 0$, which follows from $\nabla^4(r) = 0$.) Combining (2.12)–(2.17) with (1.14) allows us to calculate the integrals $L_{\parallel}$ and $L_\perp$ in terms of the invariants $M_{\parallel}$ and $M_\perp$. Of course, the result depends on the shape of the surface used in (1.14). For a spherical control surface, (1.15) tells us that

$$L_{\parallel} = (2\pi)^3\left[\tfrac{8}{15}M_{\parallel} + \tfrac{1}{15}M_\perp\right], \quad L_\perp = (2\pi)^3\left[\tfrac{9}{15}M_\perp + \tfrac{2}{15}M_{\parallel}\right], \tag{2.18}$$

from which

$$(2\pi)^3 M_{\parallel} = \tfrac{27}{14}L_{\parallel} - \tfrac{3}{14}L_\perp, \quad (2\pi)^3 M_\perp = \tfrac{12}{7}L_\perp - \tfrac{3}{7}L_{\parallel}. \tag{2.19}$$

The case of a large cylindrical control surface, of radius R and length $2H$, is somewhat more complicated. Here (1.14) yields

$$L_\parallel = 4\pi H \int_0^R \left[r_\perp \langle u_z u_z' \rangle_\infty\right]_{r_z=H} \mathrm{d}r_\perp + 4\pi R \int_0^H \left[r_z \langle u_{r_\perp} u_z' \rangle_\infty\right]_{r_\perp=R} \mathrm{d}r_z, \tag{2.20}$$

$$L_\perp = 4\pi \int_0^R \left[r_\perp^2 \langle u_{r_\perp} u_z' \rangle_\infty\right]_{r_z=H} \mathrm{d}r_\perp + 4\pi R^2 \int_0^H \left[\langle u_{r_\perp} u_{r_\perp}' \rangle_\infty\right]_{r_\perp=R} \mathrm{d}r_z, \tag{2.21}$$

and on substituting for $\langle u_i u_j' \rangle_\infty$ using (2.12)–(2.17) we find, after some algebra,

$$L_\parallel = (2\pi)^3 M_\parallel \frac{1 + \frac{1}{2}(R/H)^2}{[1 + (R/H)^2]^{3/2}} + (2\pi)^3 M_\perp \frac{\frac{1}{4}(R/H)^2}{[1 + (R/H)^2]^{3/2}}, \tag{2.22}$$

$$L_\perp = (2\pi)^3 M_\perp \left\{1 - \frac{\frac{1}{2} + \frac{3}{4}(R/H)^2}{[1 + (R/H)^2]^{3/2}}\right\} + (2\pi)^3 M_\parallel \frac{\frac{1}{2}(R/H)^2}{[1 + (R/H)^2]^{3/2}}. \tag{2.23}$$

These results confirm that $L_\parallel$ and $L_\perp$ are convergent, in the sense that they are independent of the size of V, but only conditionally so, since they depend on the ratio R/H.

Note that for $H/R \to \infty$ we obtain $L_\parallel = (2\pi)^3 M_\parallel$ and $L_\perp = (2\pi)^3 (1/2) M_\perp$, while the limit $R/H \to \infty$ yields $L_\parallel = 0$ and $L_\perp = (2\pi)^3 M_\perp$. Comparing these results with (2.10) and (2.11) we see that our dynamical invariants are

$$L_\parallel(H/R \to \infty) = (2\pi)^3 M_\parallel = \lim_{k_\perp \to 0} \int \mathrm{e}^{-j\boldsymbol{k}_\perp \cdot \boldsymbol{r}_\perp} \langle u_\parallel u_\parallel' \rangle \, \mathrm{d}\boldsymbol{r} = \text{constant}, \tag{2.24}$$

$$L_\parallel(R/H \to \infty) = \lim_{k_z \to 0} \int \mathrm{e}^{-jk_z r_z} \langle u_\parallel u_\parallel' \rangle \, \mathrm{d}\boldsymbol{r} = 0, \tag{2.25}$$

$$L_\perp(H/R \to \infty) = (2\pi)^3 \frac{1}{2} M_\perp = \lim_{k_\perp \to 0} \int \mathrm{e}^{-j\boldsymbol{k}_\perp \cdot \boldsymbol{r}_\perp} \langle \boldsymbol{u}_\perp \cdot \boldsymbol{u}_\perp' \rangle \, \mathrm{d}\boldsymbol{r} = \text{constant}, \tag{2.26}$$

and

$$L_\perp(R/H \to \infty) = (2\pi)^3 M_\perp = \lim_{k_z \to 0} \int \mathrm{e}^{-jk_z r_z} \langle \boldsymbol{u}_\perp \cdot \boldsymbol{u}_\perp' \rangle \, \mathrm{d}\boldsymbol{r} = \text{constant}. \tag{2.27}$$

Note also that, in all cases, $L_\parallel = (2\pi)^3 \Phi_\parallel(k \to 0)$ and $L_\perp = (2\pi)^3 \Phi_\perp(k \to 0)$, with $H/R \to \infty$ corresponding to $k_z = 0$ and $R/H \to \infty$ to $k_\perp = 0$.

3. Self-similarity of the large scales and possible decay laws

We now define the integral scales for axisymmetric turbulence. We introduce the integral-scale velocities in the obvious way, as $u_\parallel = \langle \boldsymbol{u}_\parallel^2 \rangle^{1/2}$ and $u_\perp = \langle (1/2)\boldsymbol{u}_\perp^2 \rangle^{1/2}$. There is, however, more ambiguity in the definition of the integral length scales. Some authors use

$$\ell_\parallel = \frac{1}{\langle \boldsymbol{u}_\perp^2 \rangle} \int \langle \boldsymbol{u}_\perp(\boldsymbol{x}) \cdot \boldsymbol{u}_\perp(\boldsymbol{x} + r\hat{\boldsymbol{e}}_z) \rangle \, \mathrm{d}r, \quad \ell_\perp = \frac{1}{\langle \boldsymbol{u}_\perp^2 \rangle} \int \langle \boldsymbol{u}_\perp(\boldsymbol{x}) \cdot \boldsymbol{u}_\perp(\boldsymbol{x} + r\hat{\boldsymbol{e}}_x) \rangle \, \mathrm{d}r, \tag{3.1}$$

while others prefer definitions in terms of longitudinal velocity correlation functions:

$$\ell_\parallel = \ell_{zz} = \frac{1}{u_z^2} \int \langle u_z(\boldsymbol{x}) u_z(\boldsymbol{x} + r\hat{\boldsymbol{e}}_z) \rangle \, \mathrm{d}r, \quad \ell_\perp = \tfrac{1}{2}(\ell_{xx} + \ell_{yy}), \tag{3.2}$$

where

$$\ell_{xx} = \frac{1}{u_x^2}\int \langle u_x(\boldsymbol{x})u_x(\boldsymbol{x}+r\hat{\boldsymbol{e}}_x)\rangle \,\mathrm{d}r, \quad \ell_{yy} = \frac{1}{u_y^2}\int \langle u_y(\boldsymbol{x})u_y(\boldsymbol{x}+r\hat{\boldsymbol{e}}_y)\rangle \,\mathrm{d}r. \tag{3.3}$$

Both (3.1) and (3.2) are equivalent (differing only by a constant factor) when the large scales evolve in a self-similar way, and we shall consider both definitions. Definition (3.2) has the advantage that it corresponds to the usual definition used in isotropic turbulence.

If the large eddies are self-similar when normalized by these integral scales, which is often a good approximation in fully developed, freely decaying turbulence, then (2.24) and (2.26) demand (Davidson 2010)

$$u_\parallel^2\ell_\perp^2\ell_\parallel = \text{constant}, \quad u_\perp^2\ell_\perp^2\ell_\parallel = \text{constant} \quad \text{(fully developed turbulence)}, \tag{3.4}$$

from which

$$u_\parallel^2/u_\perp^2 = \text{constant} \quad \text{(fully developed turbulence)}. \tag{3.5}$$

Evidently, when the large scales are self-similar, any anisotropy which is present in the initial condition will persist throughout the decay, as suggested by Chasnov (1995). This is an interesting observation as it contradicts the widely held belief that freely decaying, homogeneous turbulence should exhibit a 'return to isotropy'. However, Townsend (1976) notes that any initial anisotropy in grid turbulence is very persistent, while the grid turbulence experiments of Krogstad & Davidson (2010) and Lavoie, Djenidi & Antonia (2007) show no return to isotropy. Moreover, persistent anisotropy of $u_\parallel^2/u_\perp^2$ in axisymentric turbulence is noted in Kassinos *et al.* (2001). So (3.5) is not necessarily inconsistent with the experimental evidence. In any event, perhaps the best way to probe the validity of (3.5) is through direct numerical simulations.

We now consider the rate of energy decay under the assumption that (3.5) is correct. Since $u_\parallel^2/u_\perp^2 = \text{constant}$, we need only consider one component of energy and we choose $u_\perp^2$. Under the usual assumption that the flux of energy to small scales is controlled by the large scales, the rate of decay of $u_\perp^2$ will be some unknown function of $u_\parallel, u_\perp, \ell_\parallel$ and $\ell_\perp$. Dimensional analysis, plus the fact that $u_\parallel^2/u_\perp^2 = \text{constant}$, then gives

$$\frac{\mathrm{d}u_\perp^2}{\mathrm{d}t} = -A(\ell_\parallel/\ell_\perp)\frac{u_\perp^3}{\ell_\perp}, \tag{3.6}$$

where A is a dimensionless function of $\ell_\parallel/\ell_\perp$. Now certain, but by no means all, types of fully developed axisymmetric turbulence satisfy $u_\perp/\ell_\perp \sim u_\parallel/\ell_\parallel$ as a result of continuity. This is true, for example, of flows in which $\ell_\parallel/\ell_\perp \ll 1$ and $u_\parallel^2/u_\perp^2 \ll 1$, i.e. layers of almost horizontal turbulence, like the pancake eddies seen in strongly stratified turbulence. In such cases the constraint $u_\parallel^2/u_\perp^2 = \text{constant}$ demands that $\ell_\parallel/\ell_\perp = \text{constant}$ (in fully developed turbulence), and so (3.4) and (3.6) simplify to

$$u_\perp^2\ell_\perp^3 = \text{constant}, \quad \frac{\mathrm{d}u_\perp^2}{\mathrm{d}t} = -A\frac{u_\perp^3}{\ell_\perp}, \quad A \approx \text{constant}, \tag{3.7}$$

which is reminiscent of isotropic turbulence. Indeed, integration of (3.7) results in the isotropic-like decay laws

$$u_\perp^2 \sim u_\parallel^2 \sim t^{-6/5}, \quad \ell_\perp \sim \ell_\parallel \sim t^{2/5}, \tag{3.8}$$

at least for fully developed turbulence. However, other types of axisymmetric turbulence are not constrained by $u_\perp/\ell_\perp \sim u_\parallel/\ell_\parallel$ and in those cases (3.4) and (3.6) remain unclosed and we have no means of predicting the energy decay exponent m in $u_\parallel^2 \sim t^{-m}$ and $u_\perp^2 \sim t^{-m}$. One of the purposes of our numerical experiments is to investigate the effect of anisotropy on the exponent m.

4. The numerical evidence

In the numerical experiments which follow we put the key theoretical predictions, expressions (2.10) and (2.11), to the test. We also seek answers to the following questions.

(i) Does self-similarity of the large scales hold in fully developed, axisymmetric Saffman turbulence?

(ii) If the answer to (i) is yes, is the anisotropy persistent throughout the fully developed stages of decay, as suggested by (3.5)?

(iii) Do we recover the energy decay law (1.7) in the case of fully developed isotropic turbulence?

(iv) How do the energy decay exponents $m_\parallel$ and $m_\perp$ in $u_\parallel^2 \sim t^{-m_\parallel}$ and $u_\perp^2 \sim t^{-m_\perp}$ vary with the anisotropy, $\ell_\parallel/\ell_\perp$ and $u_\parallel^2/u_\perp^2$, and do we recover (3.8) in some cases?

(v) How are these results influenced by helicity?

Note that by 'fully developed turbulence' we mean turbulence that has largely forgotten its initial conditions, which in any event are somewhat unphysical (i.e. random phases of the Fourier modes).

The simulations reported here employ the spectral code described in Ishida *et al.* (2006). The boundary conditions are periodic and the random initial conditions were chosen from a Gaussian ensemble. The prescribed initial energy spectrum has the form $E \sim k^2 \exp[-k^2/k_p^2]$, where k_p is the wavenumber at which $E(k, t = 0)$ peaks. The phase-shift method was used for de-aliasing, in which the maximum wavenumber, k_{max}, of the retained Fourier modes is $\sim 2^{1/2}N/3$. The minimum wavenumber is $k_{min} = 1$ and time is normalized by the initial eddy turnover time, defined as $T = 1/\langle \boldsymbol{u}^2 \rangle_0^{1/2} k_p$.

The details of the various simulations are listed in table 1. Here N is the number of Fourier modes in each direction, η is the Kolmogorov scale, and $Re_\perp = u_\perp \ell_\perp/\nu$ with $\ell_\perp$ based on definition (3.1). Note that $Re_\parallel = u_\parallel \ell_\parallel/\nu$ at $t = 0$, also with $\ell_\parallel$ based on definition (3.1), is substantially larger than $Re_\perp = u_\perp \ell_\perp/\nu$ in most of the runs, lying in the range $Re_\parallel(t = 0) = 130$–$240$ for runs 1–4. Note also that the initial level of anisotropy is controlled by the value of $M_\parallel/M_\perp$, and the manner in which the initial anisotropy is imposed is discussed in the Appendix.

The logic of table 1 is as follows. The first five runs are designed to explore the influence of the initial level of anisotropy. They keep k_p constant and $Re_\perp(t = 0)$ roughly constant (except for run 5), while the initial anisotropy is varied from $u_\parallel^2/u_\perp^2 = 1$ in run 1 through to $u_\parallel^2/u_\perp^2 = 6.2$ in run 5. In all five cases $\ell_\parallel/\ell_\perp \geqslant 1$. Next, in run 6, which differs from run 3 only in the value of $Re_\perp(t = 0)$, we explore the possible influence Reynolds number. (In the isotropic decay simulations of Ishida *et al.* (2006), it was found that those runs in which the initial value of Re was less that 100 exhibited some dependence of $u^2(t)$ on Re, so we cannot rule out *a priori* the possibility of viscous effects acting directly on the large scales.) Similarly, in run 7, which differs from run 6 only in the value of k_p, we consider the possible influence of the periodic boundary conditions. Next, in runs 8–12, we explore the consequences of changing the precise form of the initial anisotropy. In particular, in run 8 we impose

https://doi.org/10.1017/jfm.2012.242 Published online by Cambridge University Press

Run	N	k_p	$k_p\eta$	$k_{max}\eta$ $(t=0)$	$\frac{u_\parallel^2(t=0)}{u_\perp^2(t=0)}$	$Re_\perp$ $(t=0)$	$E(k,t=0)$	Run intended to test the effect of:
1	512	40	0.19	0.58	1.0	104	$\sim k^2\exp(-k^2/k_p^2)$	Degree of initial anisotropy, $u_\parallel^2/u_\perp^2$
2	512	40	0.17	0.52	1.9	110	$\sim k^2\exp(-k^2/k_p^2)$	Degree of initial anisotropy, $u_\parallel^2/u_\perp^2$
3	512	40	0.16	0.49	2.6	116	$\sim k^2\exp(-k^2/k_p^2)$	Degree of initial anisotropy, $u_\parallel^2/u_\perp^2$
4	512	40	0.17	0.52	3.6	88	$\sim k^2\exp(-k^2/k_p^2)$	Degree of initial anisotropy, $u_\parallel^2/u_\perp^2$
5	512	40	0.19	0.56	6.2	58	$\sim k^2\exp(-k^2/k_p^2)$	Degree of initial anisotropy, $u_\parallel^2/u_\perp^2$
6	1024	40	0.07	0.82	2.6	156	$\sim k^2\exp(-k^2/k_p^2)$	$Re_\perp(t=0)$
7	1024	60	0.07	0.55	2.6	157	$\sim k^2\exp(-k^2/k_p^2)$	k_p
8	512	40	0.17	0.52	0.43	143	$\sim k^2\exp(-k^2/k_p^2)$	Precise form of the initial anisotropy
9	512	27	0.09	0.40	3.6	84	$\sim k^2, k<k_p$ $\sim k^{-5/3}, k>k_p$	Precise form of the initial anisotropy
10	Same as for run 5, but with the phases of the Fourier modes randomized at $t=40$.							Precise form of the initial anisotropy
11	512	40	0.13	0.39	0.76	95	$k^2\exp(-k^2/k_p^2)$	Precise form of the initial anisotropy
12	512	40	0.18	0.53	1.6	191	$k^2\exp(-k^2/k_p^2)$	Precise form of the initial anisotropy
13	512	40	0.16	0.49	0.4	132	$k^2\exp(-k^2/k_p^2)$	Possible role of helicity

TABLE 1. Parameters in the simulations.

$u_\parallel^2/u_\perp^2 = 0.4$, whereas $u_\parallel^2/u_\perp^2 \geqslant 1$ in first five cases, while in run 9 we change the shape of the initial energy spectrum. Run 10 is a variant of run 5, in which the phases of the Fourier modes are randomized at $t/T = 40$, and in runs 11 and 12 we try to mimic the effects of an axisymmetric contraction or expansion on isotropic turbulence by taking $u_\parallel^2/u_\perp^2 < 1$ and $\ell_\parallel/\ell_\perp > 1$ at $t = 0$ in run 11 (corresponding to the effect of a contraction) and $u_\parallel^2/u_\perp^2 > 1$ and $\ell_\parallel/\ell_\perp < 1$ at $t = 0$ in run 12 (corresponding to the effect of an expansion). Finally, in run 13, we explore the possible influence of helicity on the decay by repeating run 3 but with a helical initial condition.

Let us start with runs 1–5, the results o which are displayed in figures 1–4. Figure 1 shows the temporal variation of energy, integral length scales, and anisotropy in runs 1–5, with time scaled by the initial eddy turnover time, T. Note that $\ell_\parallel$ and $\ell_\perp$ are defined by (3.1), except in figure 1(g) where definition (3.2) is used. It is immediately apparent that there is a rapid transient of around 20 initial turnover times. During this initial transient the rate of dissipation of energy is modest because the smallest length scales are not fully excited. Moreover, there is a rapid drop in the level of anisotropy as measured by $u_\parallel^2/u_\perp^2$. This is contrary to (3.5) and suggests that the large scales are not self-similar during the initial transient. However, after this transient we observe some persistent residual anisotropy in which $u_\parallel^2/u_\perp^2$ is more or less constant, as predicted by (3.5), which is consistent with self-similarity of the large scales and contradicts the notion of a 'return to isotropy'. More remarkably, $\ell_\parallel/\ell_\perp$ is also more or less constant after the transient (though there is a slight variation with time). This is true whatever the initial level of anisotropy and whether $\ell_\parallel$ and $\ell_\perp$ are defined by (3.1) or (3.2). Given that $\ell_\parallel/\ell_\perp$ is more or less constant, we might expect (3.7) to apply, at least approximately, to these runs, so that Saffman's theory predicts $u_\perp^2 \sim u_\parallel^2 \sim t^{-6/5}$ and $\ell_\perp \sim \ell_\parallel \sim t^{2/5}$ (provided A in (3.7) is reasonably constant), irrespective of the level of anisotropy. Figure 1(a–d) tentatively suggests that these power laws are indeed good approximations to the decay of fully developed turbulence. To put this to the test, figure 1(a–d) is replotted in compensated form in figure 2. While there is some departure from $u_\perp^2 \sim t^{-6/5}$, presumably because A in (3.7) is not strictly constant, the $\ell_\perp \sim \ell_\parallel \sim t^{2/5}$ and $u_\parallel^2 \sim t^{-6/5}$ laws seems to be a good approximation. The primary conclusion, then, is that the $u^2 \sim t^{-6/5}$ decay law has wider application than simple isotropic turbulence.

Figure 3 shows the temporal evolution of $\Phi_\perp$ and $\Phi_\parallel$ for runs 3 and 5. Similar plots were obtained for runs 1, 2 and 4. Note in particular that $(1/2)M_\perp = \Phi_\perp(k_z = 0, k_\perp \to 0)$, $M_\perp = \Phi_\perp(k_\perp = 0, k_z \to 0)$ and $M_\parallel = \Phi_\parallel(k_z = 0, k_\perp \to 0)$ are all constant during the decay, as predicted by (2.10) and (2.11). This provides direct confirmation of Saffman's theory. Finally figure 4 shows the temporal evolution of $Re_\perp = u_\perp \ell_\perp/\nu$, $Re_\parallel = u_\parallel \ell_\parallel/\nu$ and $A(\ell_\parallel/\ell_\perp)$, the latter defined by (3.6), for runs 1–5. During the initial transient $A(\ell_\parallel/\ell_\perp)$ is small, reflecting the fact that the small scales are not fully excited, but after this transient A remains reasonably constant, though there is some variation which presumably accounts for the small departures from the $u_\perp^2 \sim t^{-6/5}$ law evident in figure 2. The magnitude of A is reasonably insensitive to the level of anisotropy.

Let us now turn to runs 6 and 7, which are designed to test the influence of $Re_\perp(t = 0)$ and k_p on the decay process. Figure 5 shows the variation of energy, integral length scales and $A(\ell_\parallel/\ell_\perp)$ in runs 3 and 6. These runs are identical except for their initial values of $Re_\perp$. As before, $u_\parallel$, $u_\perp$, $\ell_\parallel$ and $\ell_\perp$ are defined by (3.1), and $A(\ell_\parallel/\ell_\perp)$ by (3.6). It is clear that the value of $Re_\perp(t = 0)$ does not unduly influence the decay process, since the two simulations yield very similar results. Similarly, figure 6

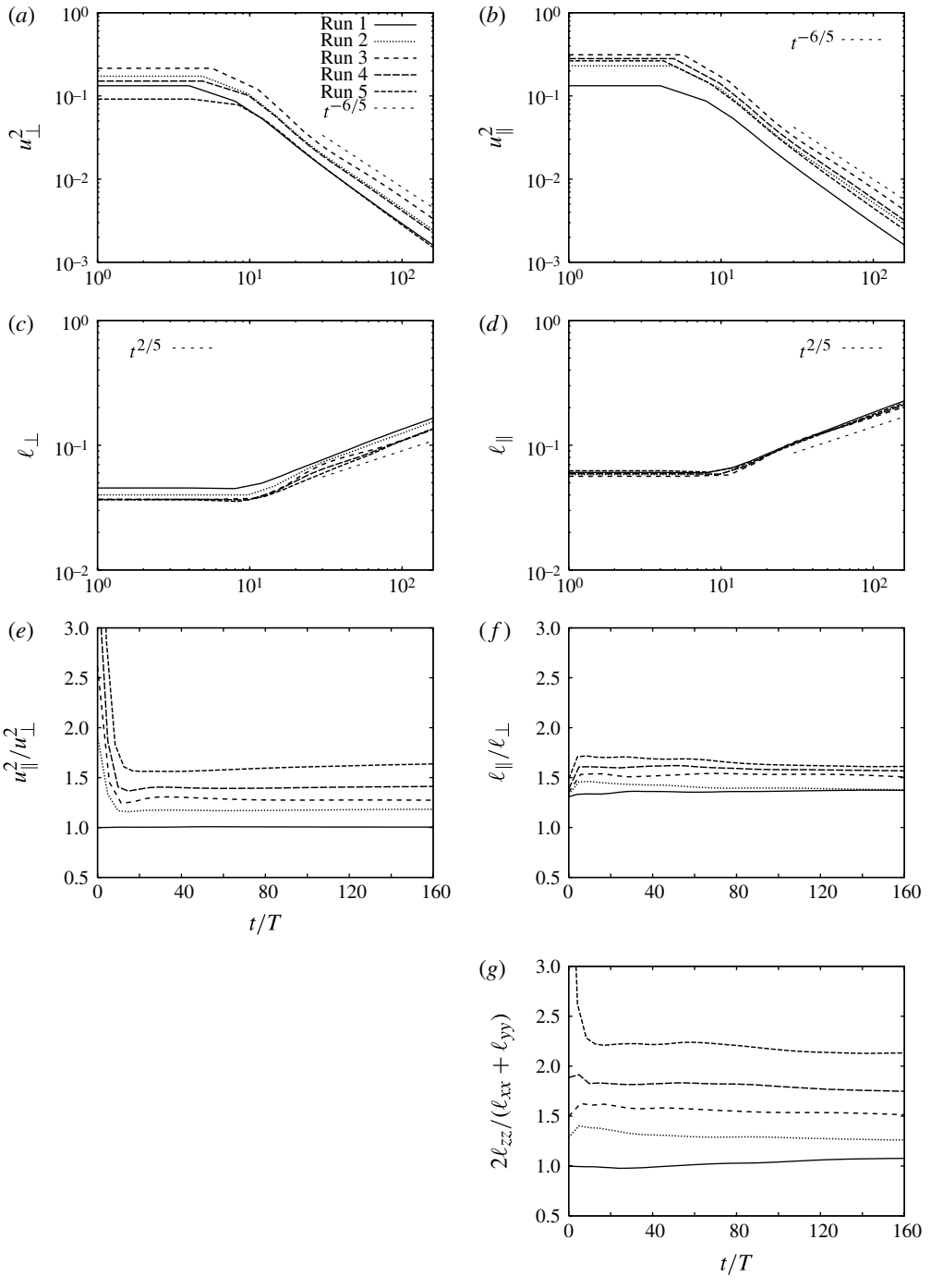

FIGURE 1. The variation of energy, integral length scales and anisotropy in runs 1–5. $\ell_\parallel$ and $\ell_\perp$ are defined by (3.1), except in (*g*) where (3.2) is used.

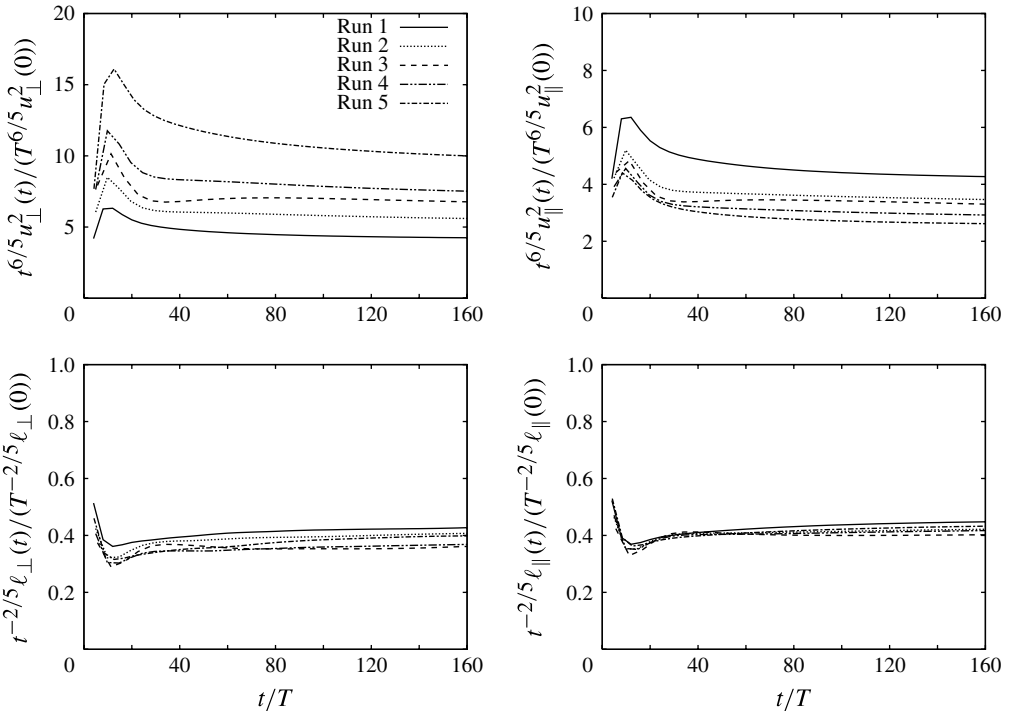

FIGURE 2. The variation of energy and integral length scales in runs 1–5 as shown in figure 1(*a–d*), but replotted in compensated form. $\ell_\parallel$ and $\ell_\perp$ are defined by (3.1).

compares runs 6 and 7, which are similar except for their values of k_p. Once again, the two runs yield similar results, and so we conclude that the computational domain is sufficiently large, relative to ℓ, for the effects of periodicity to be minimal. Figure 6 also shows plots of $\Phi_\perp$ and $\Phi_\parallel$ for run 7. As before, $(1/2)M_\perp = \Phi_\perp(k_z = 0, k_\perp \to 0)$, $M_\perp = \Phi_\perp(k_\perp = 0, k_z \to 0)$ and $M_\parallel = \Phi_\parallel(k_z = 0, k_\perp \to 0)$ are all constant during the decay, consistent with Saffman's theory.

Next we consider runs 8–12, which examine the influence of the precise form of the initial anisotropy. The results of runs 4, 8 and 9 are compared in figure 7. Recall that runs 4 and 9 are similar, except for the shape of $E(k, t = 0)$, while run 8 differs from the other simulations in that $u_\parallel^2/u_\perp^2 < 1$, so that the excess energy is now in the horizontal plane. The results for simulations 4 and 9 are very close and so, as might be expected, the precise shape of the initial energy spectrum is not very important, except of course that we require $E(k \to 0) \sim k^2$. Moreover, it is clear that in all three simulations the underlying behaviour is the same: during an initial transient there is a rapid drop in anisotropy (as measured by $u_\parallel^2/u_\perp^2$), after which the residual anisotropy becomes locked in, with both $u_\parallel^2/u_\perp^2$ and $\ell_\parallel/\ell_\perp$ more or less constant. Evidently self-similarity does not hold during the transient, since $u_\parallel^2/u_\perp^2$ is time dependent, but self-similarity is achieved after $\sim$15 turnover times. In all cases the energy and integral scales in the fully developed turbulence follow something close to Saffman's laws, $u_\perp^2 \sim u_\parallel^2 \sim t^{-6/5}$ and $\ell_\perp \sim \ell_\parallel \sim t^{2/5}$. The fact that the general behaviour is the same in all three cases suggests that the initial transient is not an artifact of the particular form of anisotropy that is imposed at $t = 0$. Rather, the initial transient is likely to

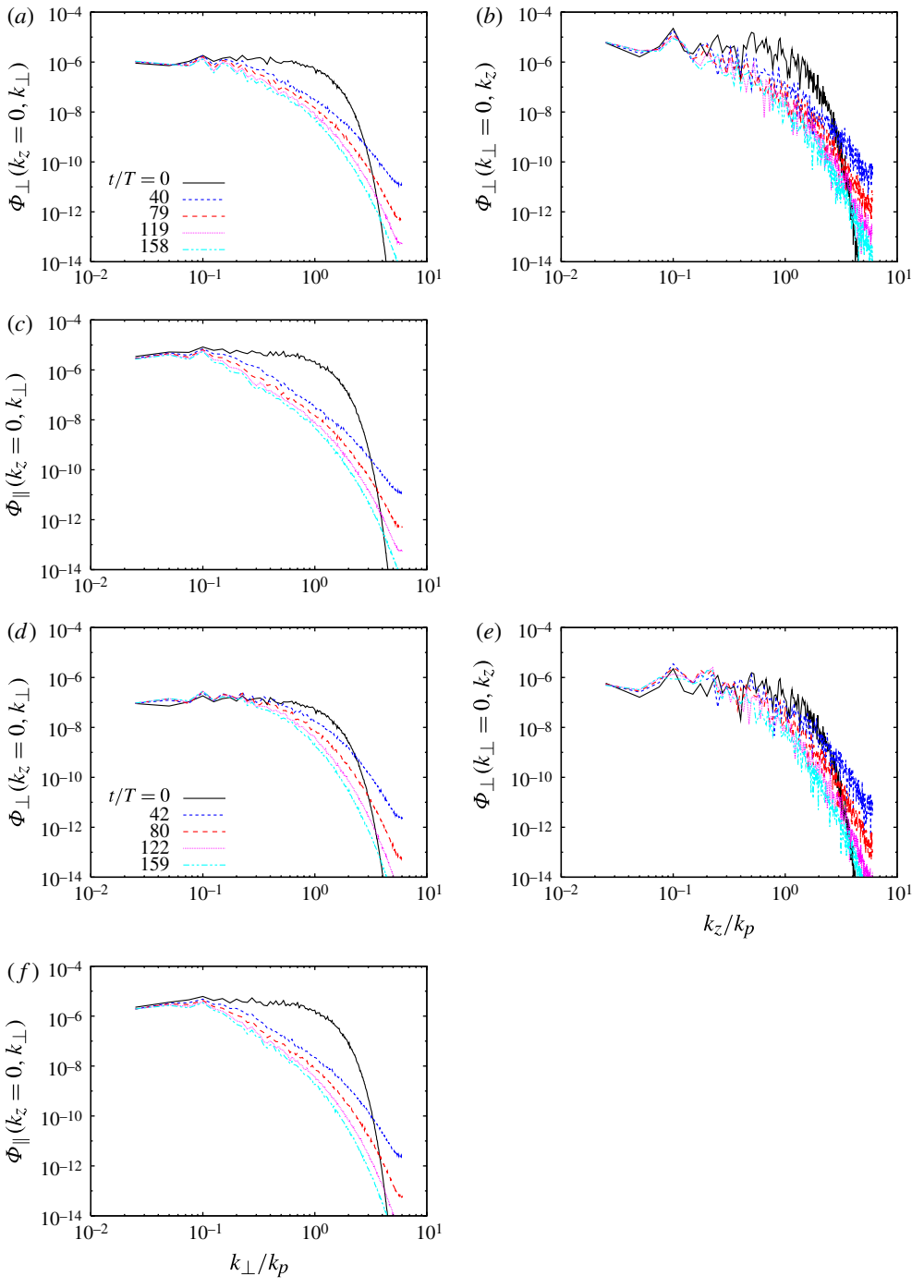

FIGURE 3. (Colour online) Plots of $\Phi_\perp$ and $\Phi_\parallel$ for runs 3 (*a–c*) and 5 (*d–f*). Note that $(1/2)M_\perp = \Phi_\perp(k_z = 0, k_\perp \to 0)$, $M_\perp = \Phi_\perp(k_\perp = 0, k_z \to 0)$ and $M_\parallel = \Phi_\parallel(k_z = 0, k_\perp \to 0)$ are all constant during the decay.

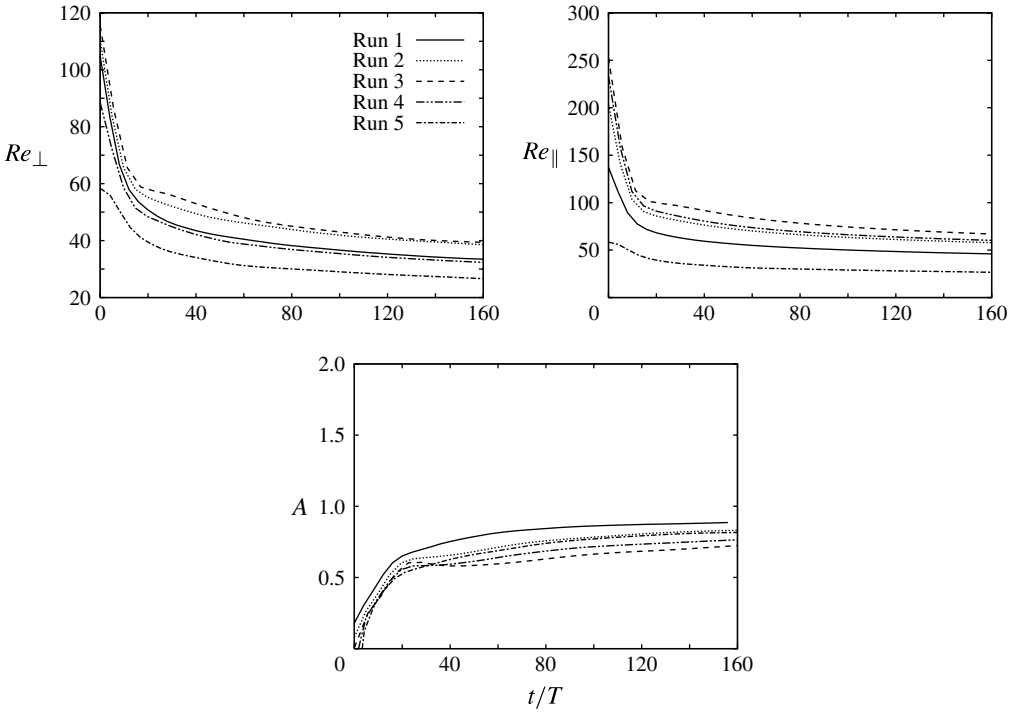

FIGURE 4. The temporal evolution of $Re_\perp = u_\perp \ell_\perp / \nu$, $Re_\parallel = u_\parallel \ell_\parallel / \nu$ and $A(\ell_\parallel/\ell_\perp)$ for runs 1–5. $A(\ell_\parallel/\ell_\perp)$ is defined by (3.6).

be a consequence of the fact that the initial conditions all have random phases and so the initial vorticity field has no structure, and it takes time for that structure to emerge through the action of the Navier–Stokes equation. If this is indeed the reason, we would not expect to see such a dramatic transient in, say, grid turbulence.

In order to test the hypothesis that randomizing the phases of the Fourier modes can cause a non-self-similar transient, run 5 was halted at $t/T = 40$ and the phases randomized. The result is shown in figure 8, labelled run 10. It can be seen that the introduction of random phases at $t/T = 40$ initiates a rapid change in $u_\parallel^2/u_\perp^2$, which constitutes a non-self-similar transient. This then settles down after around 15–20 turnover times, at which point approximate self-similarity of the large scales is once again established. As in the earlier runs, the change in $\ell_\parallel/\ell_\perp$ as a result of the transient is less marked than the change in $u_\parallel^2/u_\perp^2$. Unlike the earlier runs, however, the anisotropy increases rather than decreases during the transient. Run 10 confirms that self-similarity of the large scales is a feature of fully developed turbulence only.

The results of runs 11 and 12 are shown in figure 9. These try to mimic, in some simplistic way, the effects of an axisymmetric contraction or expansion on isotropic turbulence by taking $u_\parallel^2/u_\perp^2 < 1$ and $\ell_\parallel/\ell_\perp > 1$ at $t = 0$ in run 11 (mimicking a contraction) and $u_\parallel^2/u_\perp^2 > 1$ and $\ell_\parallel/\ell_\perp < 1$ at $t = 0$ in run 12 (mimicking an expansion). As in all previous cases, there is an initial transient after which the turbulence settles down more or less to the $u_\perp^2 \sim u_\parallel^2 \sim t^{-6/5}$ Saffman decay law. Also, as in all previous cases, the transient has a pronounced effect on the ratio $u_\parallel^2/u_\perp^2$, but less so

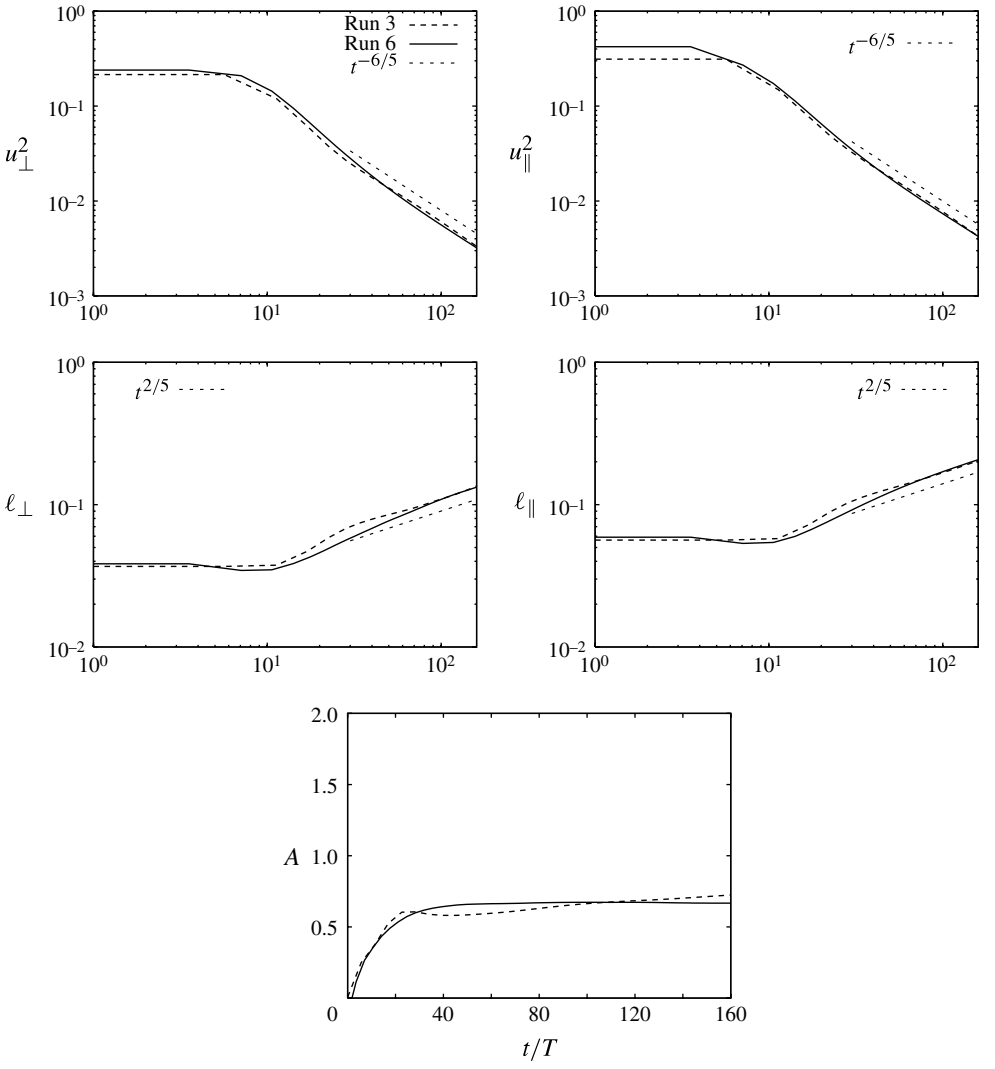

FIGURE 5. The variation of energy, integral length scales and $A(\ell_\parallel/\ell_\perp)$ in runs 3 and 6. $\ell_\parallel$ and $\ell_\perp$ are defined by (3.1) and A by (3.6).

on $\ell_\parallel/\ell_\perp$. Indeed the anisotropy, as measured by $u_\parallel^2/u_\perp^2$, reverses in both cases during the transient.

Finally, the results of run 13 are shown in figures 10 and 11, and compared with those of run 3. The initial conditions in runs 3 and 13 are similar (see table 1), except that helicity is introduced into run 13, as described in the Appendix. It is clear from figure 10, which shows the evolution of the spectra in run 13, that $(1/2)M_\perp = \Phi_\perp(k_z = 0, k_\perp \to 0)$ and $M_\parallel = \Phi_\parallel(k_z = 0, k_\perp \to 0)$ are both constant during the decay, despite the presence of helicity, as predicted in Davidson (2010). Moreover, figure 11 confirms that the presence of helicity does not fundamentally alter the general behaviour, with both $u_\parallel^2/u_\perp^2$ and $\ell_\parallel/\ell_\perp$ constant after a short transient, thus yielding a $u_\perp^2 \sim u_\parallel^2 \sim t^{-6/5}$ Saffman decay law.

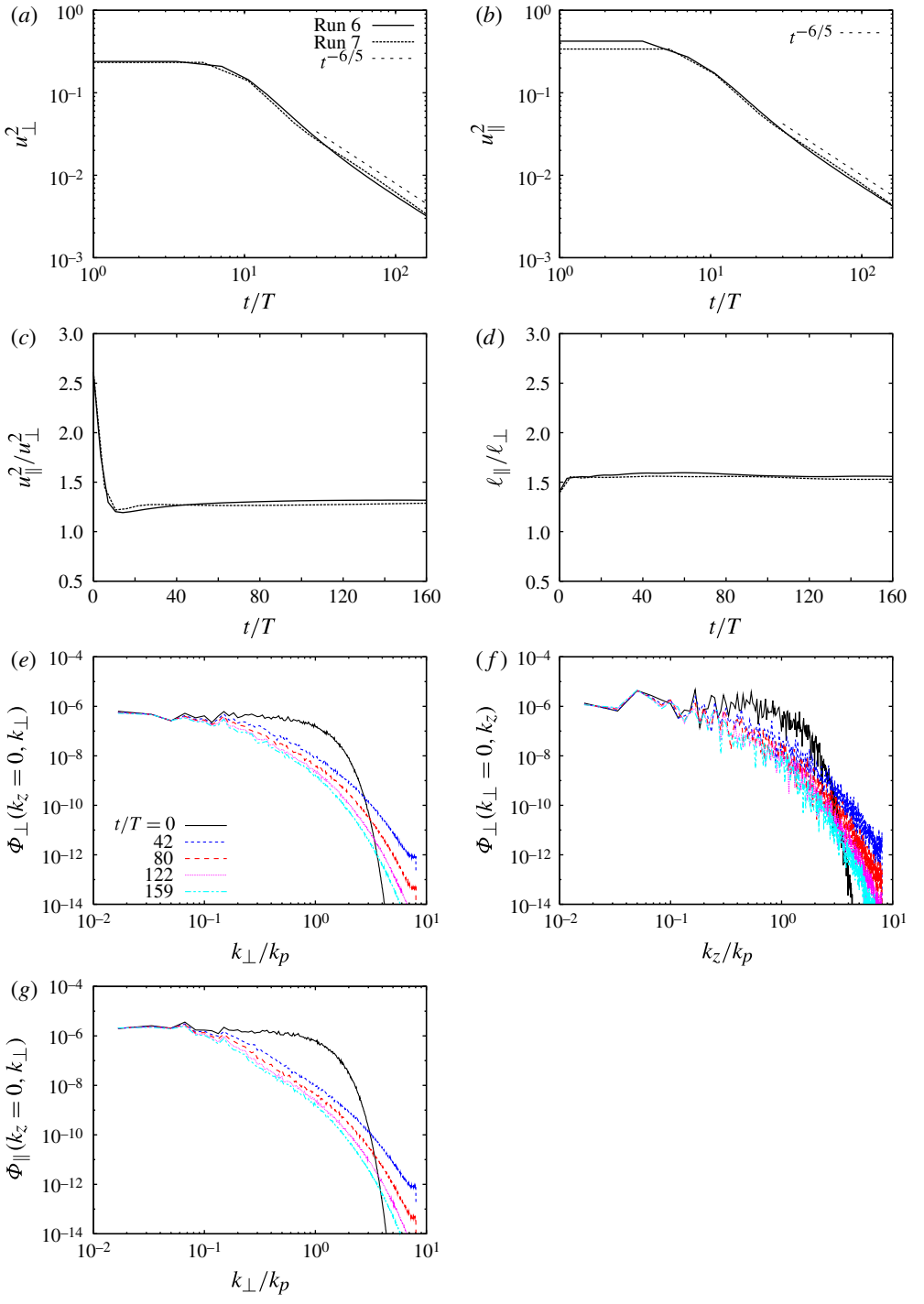

FIGURE 6. (Colour online) (*a–d*) Comparison of runs 6 and 7, which are similar except for their values of k_p. (*e–g*) Plots of $\Phi_\perp$ and $\Phi_\parallel$ for run 7. As before, $(1/2)M_\perp = \Phi_\perp(k_z = 0, k_\perp \to 0)$, $M_\perp = \Phi_\perp(k_\perp = 0, k_z \to 0)$ and $M_\parallel = \Phi_\parallel(k_z = 0, k_\perp \to 0)$ are all constant during the decay, as predicted by theory.

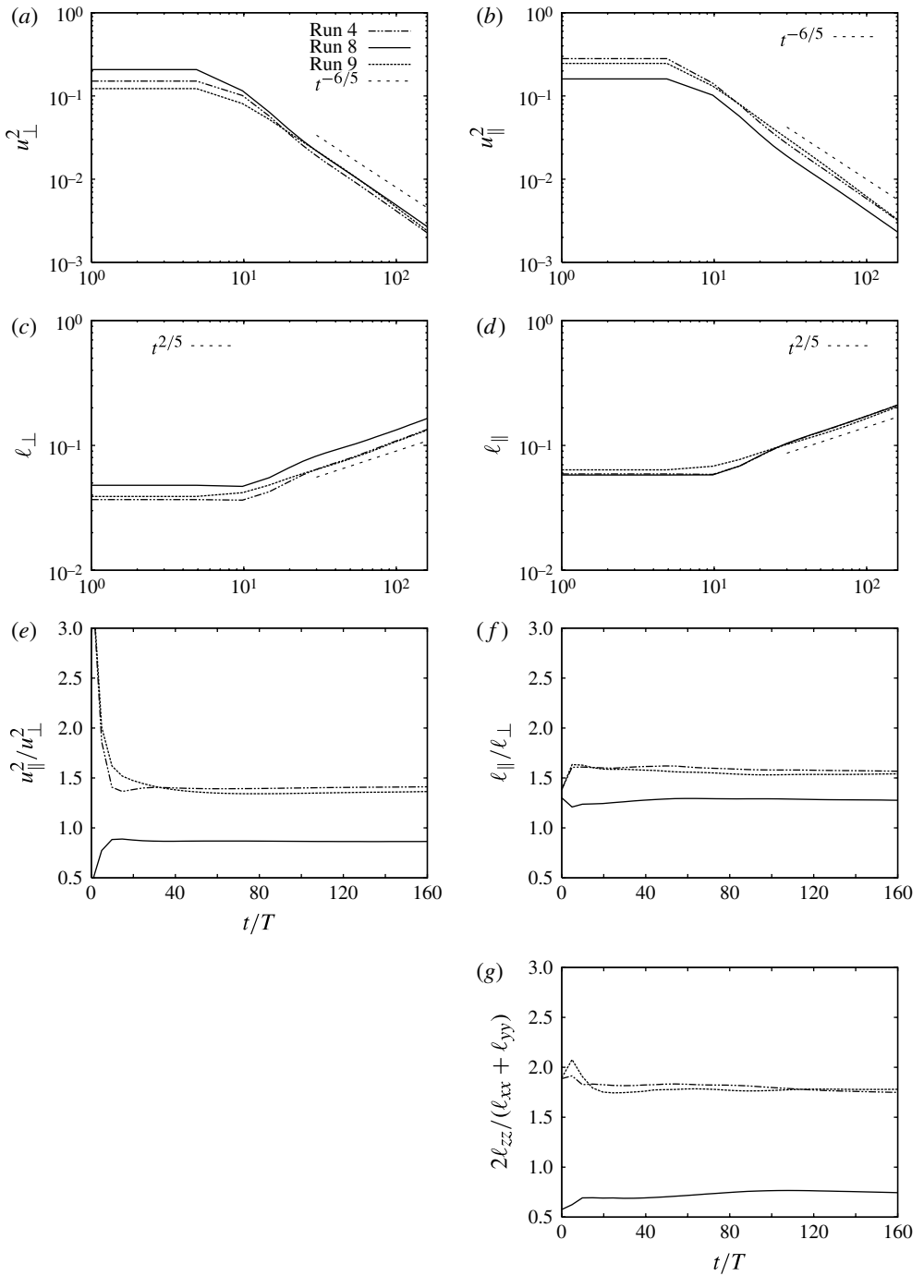

FIGURE 7. A comparison of the results of runs 4, 8 and 9. $\ell_\parallel$ and $\ell_\perp$ are defined by (3.1), except in (*g*) where the integral length scales are defined by (3.2), rather than (3.1).

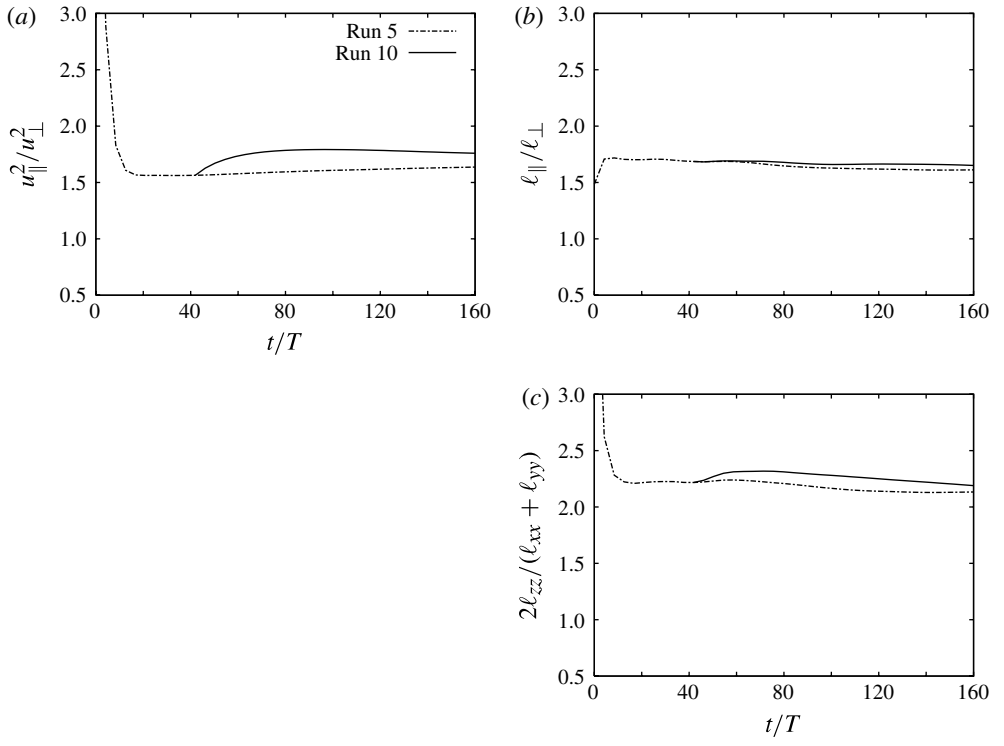

FIGURE 8. A comparison of the results of runs 5 and 10. In (*c*) the integral length scales are defined in terms of (3.2), rather than by (3.1).

5. Conclusions

We have considered freely decaying, statistically axisymmetric Saffman turbulence subject to a range of initial levels of anisotropy. Our primary interest is in the fully developed state which develops after a short transient. The numerical simulations confirm that:

(i) $M_\parallel$ and $M_\perp$ are indeed invariants of the decay;

(ii) self-similarity of the large scales holds after the initial transient;

(iii) as a consequence of (i) and (ii), $u_\parallel^2\ell_\perp^2\ell_\parallel$, $u_\perp^2\ell_\perp^2\ell_\parallel$ and $u_\parallel^2/u_\perp^2$ are all constant in the fully developed state, and so there is no return to isotropy, irrespective of the level of anisotropy;

(iv) $\ell_\parallel/\ell_\perp$ is also approximately constant in the fully developed state;

(v) as a consequence of (iii) and (iv), Saffman's decay laws, $u_\perp^2 \sim u_\parallel^2 \sim t^{-6/5}$ and $\ell_\perp \sim \ell_\parallel \sim t^{2/5}$, apply to fully developed, anisotropic turbulence.

Our findings appear to be insensitive to the initial level of anisotropy, to k_p, to $Re_\perp(t=0)$, and to the presence of helicity, at least for the range of parameters explored here.

Perhaps the most surprising finding is that $\ell_\parallel/\ell_\perp \approx$ constant in the fully developed state. This could not have been predicted in advance and is important since (3.6) then demands $u_\perp^2 \sim u_\parallel^2 \sim t^{-6/5}$, irrespective of the level of anisotropy.

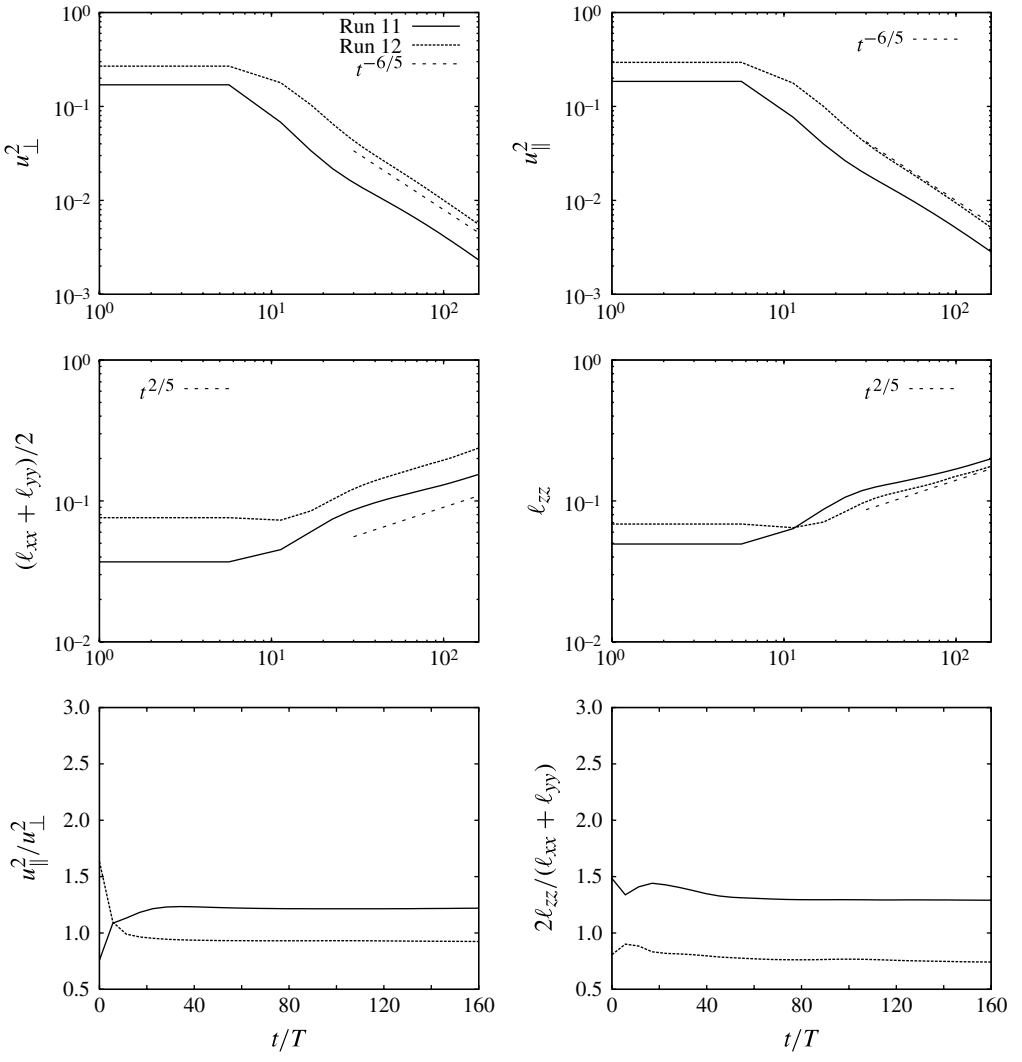

FIGURE 9. The results of runs 11 and 12. Note the reversal of the ratio $u_\parallel^2/u_\perp^2$ in both cases during the initial transient. The integral length scales are defined by (3.2).

Acknowledgements

The simulations were performed on the Earth Simulator. This work was partly supported by the Grant-in-Aid for Scientific Research (S) 20224013 from the Japan Society for the Promotion of Science (JSPS).

Appendix. The initial conditions used in the numerical simulations

The initial field $\boldsymbol{u}$ in all of the runs except run 13 may be written in the form,

$$\boldsymbol{u} = \boldsymbol{u}^{(i)} + \boldsymbol{u}^{(a)}, \tag{A 1}$$

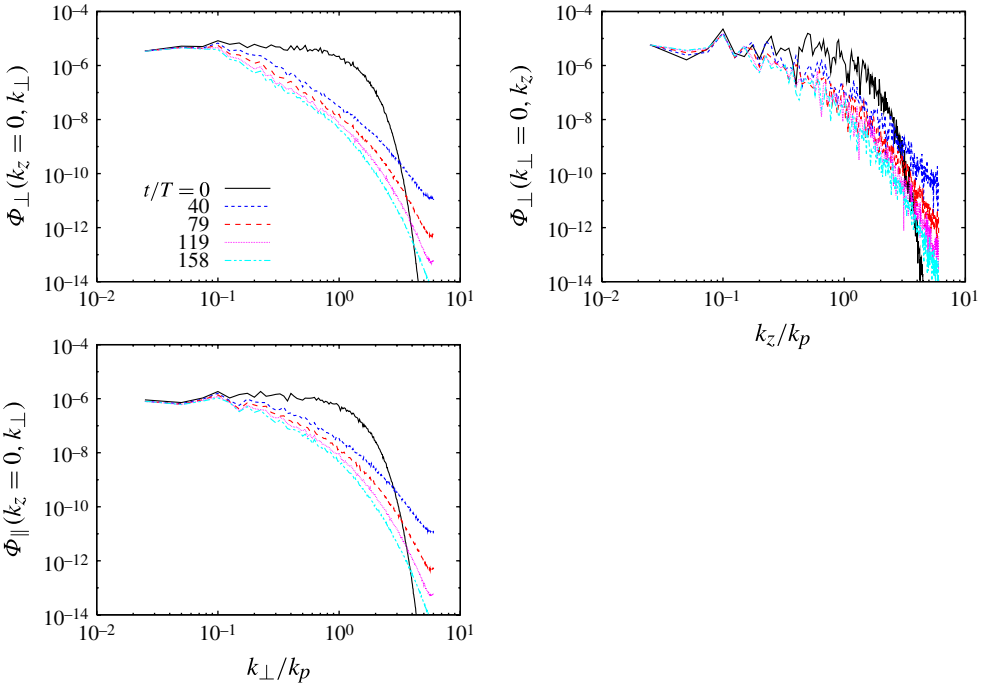

FIGURE 10. (Colour online) Plots of the evolution of $\Phi_\perp$ and $\Phi_\parallel$ for run 13. Note that $(1/2)M_\perp = \Phi_\perp(k_z = 0, k_\perp \to 0)$ and $M_\parallel = \Phi_\parallel(k_z = 0, k_\perp \to 0)$ are both constant during the decay, despite the presence of helicity, as predicted in Davidson (2010).

where $\boldsymbol{u}^{(i)}$ and $\boldsymbol{u}^{(a)}$ are respectively statistically isotropic and anisotropic components, whose Fourier transforms are given by

$$\hat{u}_i^{(i)}(\boldsymbol{k}) = D_{ij}(\boldsymbol{k})i_j(\boldsymbol{k}), \quad \hat{u}_i^{(a)}(\boldsymbol{k}) = D_{ij}(\boldsymbol{k})a_j(\boldsymbol{k}), \tag{A 2}$$

in which $D_{ij}(\boldsymbol{k}) \equiv \delta_{ij} - k_i k_j/k^2$. Here $i_j(\boldsymbol{k})$ and $a_j(\boldsymbol{k})(j = 1, 2, 3)$ are Gaussian random numbers with zero mean and independent from each other. They satisfy

$$\langle i_i(\boldsymbol{k})i_j(\boldsymbol{p})\rangle = \delta_{ij}I(k)\delta(\boldsymbol{k}+\boldsymbol{p}), \tag{A 3a}$$

$$\langle a_1(\boldsymbol{k})a_1(\boldsymbol{p})\rangle = \langle a_2(\boldsymbol{k})a_2(\boldsymbol{p})\rangle = A(\boldsymbol{k})\delta(\boldsymbol{k}+\boldsymbol{p}), \quad \langle a_3(\boldsymbol{k})a_3(\boldsymbol{p})\rangle = B(\boldsymbol{k})\delta(\boldsymbol{k}+\boldsymbol{p}), \tag{A 3b}$$

$$\langle a_i(\boldsymbol{k})a_j(\boldsymbol{p})\rangle = 0 \quad \text{if } i \neq j, \tag{A 3c}$$

as well as the reality conditions $i_i(\boldsymbol{k}) = i_i^*(-\boldsymbol{k})$, $b(\boldsymbol{k}) = b^*(-\boldsymbol{k})$. In these expressions $\delta(\boldsymbol{k}+\boldsymbol{p}) = 1$ if $\boldsymbol{k}+\boldsymbol{p} = 0$, and $\delta(\boldsymbol{k}+\boldsymbol{p}) = 0$ otherwise, * denotes the complex conjugate, and $I(\boldsymbol{k})$ is a function of only $k = |\boldsymbol{k}|$, whereas $A(\boldsymbol{k})$ and $B(\boldsymbol{k})$ are functions of only k and $\cos\theta = k_3/k$.

The initial velocity correlation spectrum $\Phi_{ij}(\boldsymbol{k}) \equiv \langle \hat{u}_i(\boldsymbol{k})\hat{u}_j(-\boldsymbol{k})\rangle$ is then given by

$$\Phi_{ij}(\boldsymbol{k}) \equiv D_{ij}(\boldsymbol{k})I(k) + [D_{i1}(\boldsymbol{k})D_{j1}(\boldsymbol{k}) + D_{i2}(\boldsymbol{k})D_{j2}(\boldsymbol{k})]\,A(\boldsymbol{k}) + D_{i3}(\boldsymbol{k})D_{j3}(\boldsymbol{k})B(\boldsymbol{k}). \tag{A 4}$$

If we put

$$I + A - (B - A)\cos^2\theta = [F + G]k^2, \quad B - A = -Gk^2, \tag{A 5}$$

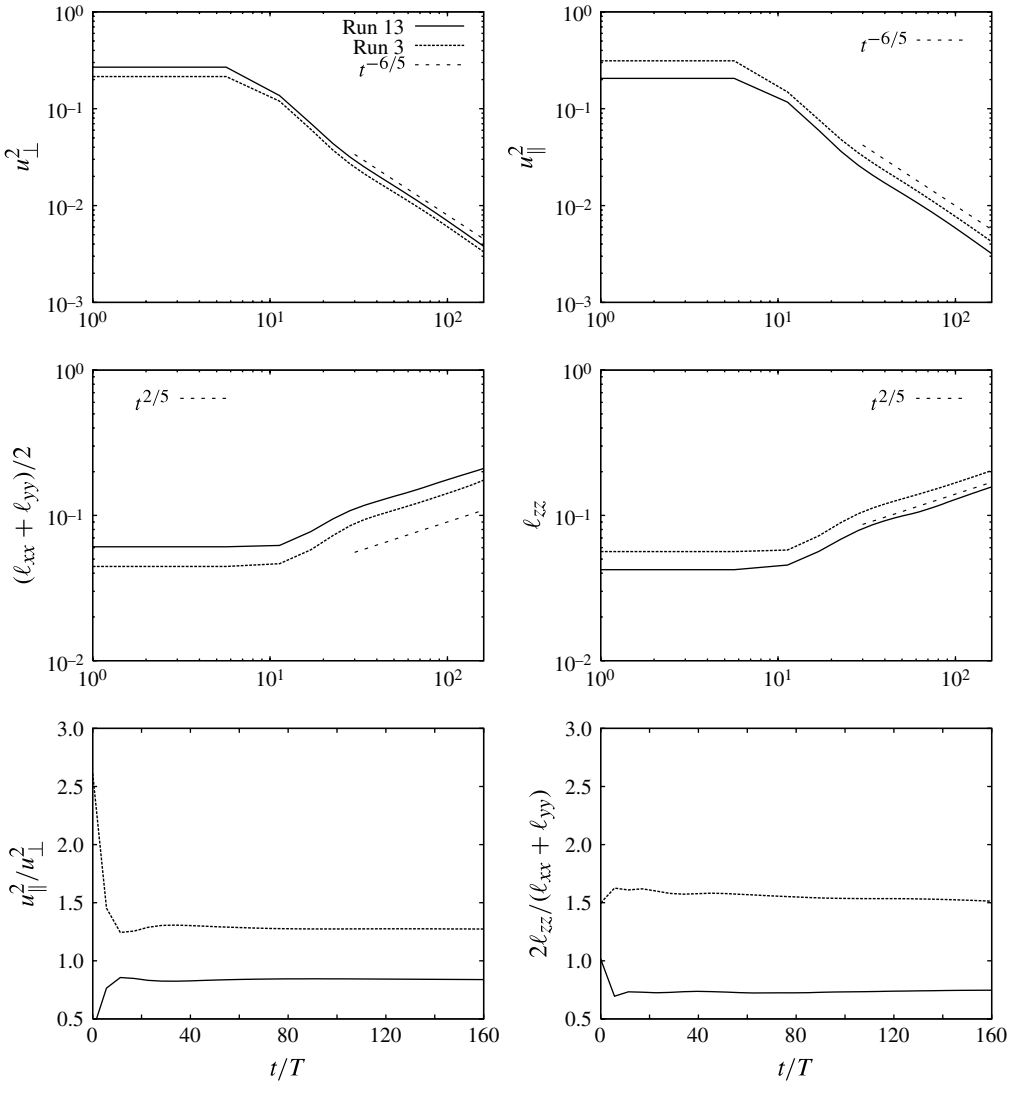

FIGURE 11. A comparison of the results of run 3 (which has no helicity) with those of run 13 (which has finite helicity). The integral length scales are defined by (3.2).

or equivalently,

$$G = (A - B)/k^2, \quad F = [(I + A) - (B - A)\cos^2\theta)]/k^2 + (B - A)/k^2, \tag{A 6}$$

then (A 4) is shown to be equivalent to (2.1).

Suppose that an impulsive force parallel to the z-axis (x_3-axis) is applied at $t = 0$ to a statistically isotropic field $\boldsymbol{u}^{(i)}$. Then the velocity field $\boldsymbol{u}$ at $t = 0^+$ is given by (A 1)–(A 3) with $A(\boldsymbol{k}) = 0$, provided that the force is statistically homogeneous and axisymmetric with respect to the symmetry axis.

In runs 1–9, we put

$$I(k) = C_I c(k, 1), \quad A(\boldsymbol{k}) = C_A c(k, 1), \quad B(\boldsymbol{k}) = C_B c(k, 1), \tag{A 7}$$

	Run 1	Run 2	Run 3, 6, 7	Run 4, 9	Run 8	Run 5
C_I	1	1	1	0.5	0.5	0.1
C_A	0	0	0	0	1.5	0
C_B	0	1.5	3	3	0	3

TABLE 2. Choice of C_I, C_A and C_B for runs 1–9.

where

$$c(k,\alpha) = \frac{1}{2\pi^{3/2}k_p^3}\exp(-\alpha k^2/k_p^2), \tag{A 8}$$

for runs 1–8, whereas $c(k,1)$ in (A 7) is replaced by

$$c(k) = \begin{cases} \gamma^2 & (k \leqslant k_p) \\ \gamma^2 k_p^{11/3} k^{-11/3} & (k \geqslant k_p) \end{cases} \tag{A 9}$$

in run 9, in which γ is a normalization constant so chosen that the total fluctuating kinetic energy is 0.5. The ratios of the three constants C_I, C_A and C_B in (A 8) determine the degree of the initial anisotropy, and were chosen as in table 2.

In runs 11–12, we put

$$I(k) = 0, \quad A(\boldsymbol{k}) = C_A c(k,\alpha), \quad B(\boldsymbol{k}) = C_B c(k,\beta), \tag{A 10}$$

where $c(k,\alpha)$ is given by (A 8), and

$$C_A = 1/2, \quad C_B = 3/2, \quad \alpha = (2/9)^{2/3}, \quad \beta = 1, \tag{A 11}$$

for run 11, and

$$C_A = 3, \quad C_B = 3/2, \quad \alpha = 4^{2/3}, \quad \beta = 1, \tag{A 12}$$

for run 12. The initial fields of runs 11 and 12 satisfy $u_\parallel^2/u_\perp^2\langle 1, \ell_\parallel/\ell_\perp\rangle 1$, and $u_\parallel^2/u_\perp^2 > 1$, $\ell_\parallel/\ell_\perp < 1$, respectively.

The initial velocity field of run 13 is generated by taking the vector product of the initial velocity field of run 3:

$$\hat{\boldsymbol{u}}(\boldsymbol{k}) \times \mathrm{i}\boldsymbol{k}/k \tag{A 13}$$

in the wave vector space, where i is the imaginary unit.

Note that (A 4) with (A 7) gives

$$\Phi_{ii}(\boldsymbol{k}) = \left[2C_I + C_A\left(2 - \frac{k_1^2+k_2^2}{k^2}\right) + C_B\left(1 - \frac{k_3^2}{k^2}\right)\right] c(k,1). \tag{A 14}$$

The invariants M_{ij}, $M_\parallel$ and $M_\perp$ in (1.9) and (2.3) are then given by

$$M_{ij}/c(0,1) = (C_I + C_B)\delta_{i3}\delta_{j3} + (C_I + C_A)(\delta_{i1}\delta_{j1} + \delta_{i2}\delta_{j2}), \tag{A 15}$$

$$M_\parallel/c(0,1) = C_I + C_B, \quad M_\perp/c(0,1) = 2C_A + 2C_I, \tag{A 16}$$

at $t = 0$.

REFERENCES

BATCHELOR, G. K. & PROUDMAN, I. 1956 The large-scale structure of homogenous turbulence. *Phil. Trans. R. Soc. Lond.* A **248**, 369–405.

BENNETT, J. C. & CORSSIN, S. 1978 Small Reynolds number nearly isotropic turbulence in a straight duct and a contraction. *Phys. Fluids* **21** (12), 2129–2140.

CHASNOV, J. R. 1995 The decay of axisymmetric homogeneous turbulence. *Phys. Fluids* **7** (3), 600–605.

DAVIDSON, P. A. 2004 *Turbulence: an Introduction for Scientists and Engineers*. Oxford University Press.

DAVIDSON, P. A. 2009 The role of angular momentum conservation in homogeneous turbulence. *J. Fluid Mech.* **632**, 329–358.

DAVIDSON, P. A. 2010 On the decay of Saffman turbulence subject to rotation, stratification, or an imposed magnetic field. *J. Fluid Mech.* **663**, 268–292.

DAVIDSON, P. A. 2011 The minimum energy decay rate in quasi-isotropic grid turbulence. *Phys. Fluids* **23**, 085108.

ISHIDA, T., DAVIDSON, P. A. & KANEDA, Y. 2006 On the decay of isotropic turbulence. *J. Fluid Mech.* **564**, 455.

KASSINOS, S. C., REYNOLDS, W. C. & ROGERS, M. M. 2001 One-point turbulence structure tensors. *J. Fluid Mech.* **428**, 213–248.

KROGSTAD, P.-A. & DAVIDSON, P. A. 2010 Is grid turbulence Saffman turbulence? *J. Fluid Mech.* **642**, 373–394.

LAVOIE, P., DJENIDI, L. & ANTONIA, R. A. 2007 Effects of initial conditions in decaying turbulence generated by passive grids. *J. Fluid Mech.* **585**, 395–420.

SAFFMAN, P. G. 1967*a* The large-scale structure of homogeneous turbulence. *J. Fluid Mech.* **27** (3), 581–593.

SAFFMAN, P. G. 1967*b* Note on decay of homogeneous turbulence. *Phys. Fluids* **10** (6), 1349.

TOWNSEND, A. A. 1976 *The Structure of Turbulence Shear Flow*. Cambridge University Press.